crystals

MDPI

Article

Sustainable Production and Physicochemical Characteristics of Calcium Sulfate Dihydrate Prepared from Waste Eggshells

Somkiat Seesanong [1], Chaowared Seangarun [2], Banjong Boonchom [2,3,4,*], Nongnuch Laohavisuti [5,*], Wimonmat Boonmee [6], Pesak Rungrojchaipon [4] and Phairat Phimsirikul [1]

[1] Office of Administrative Interdisciplinary Program on Agricultural Technology, School of Agricultural Technology, King Mongkut's Institute of Technology Ladkrabang, Bangkok 10520, Thailand; somkiat.se@kmitl.ac.th (S.S.); phirat.ph@kmitl.ac.th (P.P.)
[2] Material Science for Environmental Sustainability Research Unit, School of Science, King Mongkut's Institute of Technology Ladkrabang, Bangkok 10520, Thailand; chaowared@gmail.com
[3] Municipal Waste and Wastewater Management Learning Center, School of Science, King Mongkut's Institute of Technology Ladkrabang, Bangkok 10520, Thailand
[4] Department of Chemistry, School of Science, King Mongkut's Institute of Technology Ladkrabang, Bangkok 10520, Thailand; pesak.ru@kmitl.ac.th
[5] Department of Animal Production Technology and Fishery, School of Agricultural Technology, King Mongkut's Institute of Technology Ladkrabang, Bangkok 10520, Thailand
[6] Department of Biology, School of Science, King Mongkut's Institute of Technology Ladkrabang, Bangkok 10520, Thailand; wimonmat.bo@kmitl.ac.th
* Correspondence: banjong.bo@kmitl.ac.th (B.B.); nongnuch.la@kmitl.ac.th (N.L.)

Abstract: Gypsum products (calcium sulfate dihydrate, $CaSO_4 \cdot 2H_2O$) were synthesized through an eco-friendly and low-cost process by two different renewable calcium carbonate sources ($CaCO_3$), hen and duck eggshell wastes, with product yields obtained of 84.73 and 87.74%, respectively. The X-ray fluorescence results indicated that calcium oxide (CaO) and sulfur trioxide (SO_3) are the major elemental components of $CaSO_4 \cdot 2H_2O$ prepared from both calcium sources. The Fourier transform infrared results confirmed the vibrational characteristics of SO_4^{2-} and H_2O functional groups in the chemical structure of the prepared samples. The X-ray diffraction patterns of $CaSO_4 \cdot 2H_2O$ prepared from both calcium sources confirmed the sample's crystal structure as well as the chemical formula, after comparing them to the standard powder diffraction file. The crystallite sizes of $CaSO_4 \cdot 2H_2O$ products were calculated from the experimental diffraction peak through the Scherrer equation and found to be 19–20 nm. The positive preferential growth (*Pg*) value highlighted the excellent stability of the synthesized $CaSO_4 \cdot 2H_2O$. The scanning electron microscopic results showed the agglomeration particles of hen- and duck-$CaCO_3$ raw agents, whereas plate-like particles were observed for hen- and duck-$CaSO_4 \cdot 2H_2O$ products but the particle sizes were different.

Keywords: eco-friendly preparation; calcium sulfate; gypsum; eggshell waste; renewable material; sustainability

Citation: Seesanong, S.; Seangarun, C.; Boonchom, B.; Laohavisuti, N.; Boonmee, W.; Rungrojchaipon, P.; Phimsirikul, P. Sustainable Production and Physicochemical Characteristics of Calcium Sulfate Dihydrate Prepared from Waste Eggshells. *Crystals* **2024**, *14*, 577. https://doi.org/10.3390/cryst14070577

Academic Editor: Fan Yang

Received: 15 May 2024
Revised: 6 June 2024
Accepted: 16 June 2024
Published: 21 June 2024

1. Introduction

Calcium sulfate, a ceramic material, is widely used for various applications. It has been used as a binder material for building construction [1], bone graft material [2], periodontal disease treatment [3], endodontic lesions [4], alveolar bone loss [5], maxillary sinus augmentation [6], filler for plastic [7] and rubber [8], coating [9], desiccant [10], coagulant [11], catalyst [12], and bleaching agent [13]. Four calcium sulfate forms have been observed and previously reported: calcium sulfate dihydrate ($CaSO_4 \cdot 2H_2O$, gypsum) [13], α- and β-calcium sulfate hemihydrate ($CaSO_4 \cdot 0.5H_2O$, bassanite) [14], and calcium sulfate anhydrous ($CaSO_4$, anhydrite) [15]. Moreover, two different anhydrous polymorphs, β-$CaSO_4$ (insoluble anhydrite, natural anhydrite form) and γ-$CaSO_4$ (soluble anhydrite), were also reported [16]. The phase transformation, crystal structure, morphology, and growth

rate of calcium sulfate depend on different physicochemical conditions, i.e., temperature, pressure, solutions, and other ionic minerals [17,18]. Calcium sulfates can be obtained from different preparation processes, i.e., formed from an aqueous sulfuric acid [19], flue gas desulfurization [20], reverse microemulsion [21], and chemical precipitation [22]. In turn, their characteristics (color, hardness, and density), crystal structure, solubility, optical property (translucence and refractive index), and applications depend on the preparation conditions [18].

Eco-friendly production and consumption for sustainable development are considered important topics. Furthermore, the depletion of the environment is intensifying the need to reduce pollution. In that context, "sustainability" is related to the reliability of resources and ecology, which connects to society, economies, and environments. At present, one-third of the total food we produce is cast off as waste, and this waste affects the environment [23]. Accordingly, the utilization of waste food may form part of the approach to ensuring a sustainable environment. Waste eggshells are one of the most discarded foods, generated from consumption as well as from various industries, i.e., drugs, cosmetics, etc. They offer an important calcium source since the main component of eggshells is calcium carbonate ($CaCO_3$), which varies from 95 to 97% [24], mainly in the form of calcite polymorph > 94 wt%, which is considered a rich natural calcium source [25].

Eggshells have been applied in various fields of materials science, mostly with industrial and biomedical applications [26]. Meng and Deng [27] demonstrated a novel application of waste eggshells as a multifunctional reaction system to regulate the reactants and solution pH. They proposed the idea of transferring waste eggshells into a unique reaction system for the synthesis of Co_9S_8 nanorod arrays. Furthermore, due to its pore structure, eggshell is an excellent secondary raw material for the preparation of value-added products with a fine powder, such as porous solid catalysts [26]. Since the main chemical component of eggshells is $CaCO_3$, which can then be calcined, CaO may be obtained, one of the most promising metal oxides with high basicity. This basicity property highlights that eggshell-derived CaO can be used as a heterogeneous catalyst in biodiesel production [28]. Previously, eggshell was applied as an adsorbent for the removal of hydrogen sulfide (H_2S) from wastewater [29]. Additionally, eggshells are very useful green and economic adsorbents due to their availability and absence of toxic elements. Another novel application of eggshell waste is as a calcium (Ca^{2+}) source to prepare hydroxyapatite (a calcium phosphate ceramic material with the chemical formula $Ca_{10}(PO_4)_6(OH)_2$) [30]. This calcium phosphate form, hydroxyapatite, has been applied as a biomaterial for bone and dental replacement because of its natural characteristics and its incorporation into bone tissues [31]. Moreover, beyond those already reported, the use of food waste for the production of other compounds will also help reduce the pollution effect of waste on the environment, with the subsequent conversion of the waste into a highly valuable product having the added benefit of reducing the production cost of that product.

In addition to the preparation of hydroxyapatite, the use of eggshells has also been reported as a secondary material for the preparation of other important agricultural- and chemical-based compounds, i.e., monocalcium phosphate ($Ca(H_2PO_4)_2{\cdot}H_2O$), dicalcium phosphate ($CaHPO_4{\cdot}2H_2O$), and tricalcium phosphate ($Ca_3(PO_4)_2$) [32]. Eggshell was also used as a Ca^{2+} source in the preparation of calcium sulfate compounds, e.g., $CaSO_4{\cdot}2H_2O$ (gypsum) [23], which is an important fertilizer that provides Ca^{2+} and SO_4^{2-} nutrients for plants. Gypsum is obtained from two sources: natural and synthetic gypsums. Synthetic gypsum is produced as a waste product or by-product in a range of industrial processes. Recently, a study reported the synthesis of gypsum from a reaction between bassanite, eggshells, and Pila globosa shells with sulfuric acid, which was carried out with different process conditions, acid concentrations, and time lengths [23,24,26–29].

Egg production in Thailand displays significant growth. According to the statistical data reported by the Information and Communication Technology Center (Department of Livestock Development, Ministry of Agriculture and Cooperatives, Thailand), in 2022, Thailand had more than 66 and 17 million hens and ducks, which produced more than 51 and

12 million hen and duck eggs per day, respectively. These quantities create lots of hen and duck eggshell waste. Against that background, the synthesis of value-added compounds from renewable natural resources is the driving force for environmental sustainability. Bringing the two together, this work aimed to use bio-waste eggshells as raw materials (a Ca^{2+} source) for the preparation of valuable products ($CaSO_4 \cdot 2H_2O$) for environmental sustainability, specifically products to be used as soil treatments and fertilizers. The demand for fertilizer is greatly influenced by the demand for food, which is ever-growing due to the significantly increasing global population. $CaSO_4 \cdot 2H_2O$ is suitable to use as a fertilizer component as it is 150 times more soluble in water than $CaCO_3$ and is used to minimize crusting, lessen erosion, and reduce phytotoxicity, as well as to treat sodium-enriched soil [23]. In this study, the physicochemical characteristics of $CaSO_4 \cdot 2H_2O$ samples were investigated by using X-ray fluorescence (XRF, an analytical technique used to determine the elemental composition of the samples), X-ray diffraction (XRD, a technique used for phase identification of the samples), Fourier-transform infrared (FTIR) spectroscopy (a technique used to record an infrared spectrum of absorption or transmission of the samples and confirm the presence of the functional groups), and scanning electron microscopy (SEM, a type of electron microscope that photographs the morphology of a sample by scanning the surface with a focused beam of electrons). This article reports an easy and low-cost process of using two different renewable calcium carbonate sources ($CaCO_3$)—hen and duck eggshell wastes—to produce cheap gypsum products to be used in the agroindustry.

2. Experiments

2.1. Materials and their Synthesis

Distilled water prepared by the Department of Chemistry, School of Science, King Mongkut's Institute of Technology Ladkrabang, Thailand was used throughout this study. Sulfuric acid (H_2SO_4, 98% *w*/*w*, 18 mol/L, AR grade) was purchased from Sigma-Aldrich. Hen and duck eggshells were collected from the bakery shops and canteens at the School of Science. Each eggshell type (duck or hen) was random, soaked, and cleaned with tap and distilled water several times, exposed to sunlight under ambient air for 2 days (drying), and ground with a 450 rpm ball milled process (MTI Corporation, Richmond, CA, USA, TMAX-XQM planetary ball milling) for 120 min using binary mixtures of two zirconium oxide (ZrO_2) ball sizes (2 and 10 mm) under dry conditions with an eggshell:ball weight ratio of 1:10, creating hen- or duck-eggshell $CaCO_3$ powders.

For the preparation of calcium sulfate, concentrated H_2SO_4 (18 mol/L, 98% *w*/*w*) was first diluted with distilled water to prepare 10 mol/L (~54% *w*/*w*), and diluted H_2SO_4 was then used as the $SO_4{}^{2-}$ source, whereas the eggshell powder was used as the Ca^{2+} source ($CaCO_3$). We gradually added 20 mL of diluted H_2SO_4 solution (~0.2 mole) to 20 g of each $CaCO_3$ (~0.2 mole) powdered from duck or hen eggshell. This created a molar ratio between the eggshell powder and H_2SO_4 of 1:1. The preparation reaction was conducted under ambient conditions without temperature control. The mixed suspension was stirred (C-MAG HS 7, IKA magnetic stirrer, Staufen, Germany) at 100 rpm until no more carbon dioxide (CO_2) evolved. Equation (1) demonstrates the chemical reaction between H_2SO_4 solution and eggshell $CaCO_3$ powder, which is the same reaction as in previous research [23,24,26–29] but the process conditions, acid concentration, and time consumption are different.

$$H_2SO_4(aq) + CaCO_3(s) \rightarrow Ca^{2+}(aq) + SO_4{}^{2-}(aq) + nH_2O(l) + CO_2(g)\uparrow \quad (1)$$

The calcium sulfate product (calcium sulfate hydrate, $CaSO_4 \cdot nH_2O$) was precipitated in a powder form, as demonstrated in Equation (2), when the solvent (H_2O) was evaporated in an oven (Binder FD 115) at 60 °C for 48 h.

$$Ca^{2+}(aq) + SO_4{}^{2-}(aq) \rightarrow CaSO_4 \cdot nH_2O(s) + mH_2O(g)\uparrow \quad (2)$$

No additional chemicals were used in the calcium sulfate formation, ensuring a sustainable development by avoiding unnecessary precipitating reagents. The usage of waste eggshells as a raw reacting material also supports the sustainable production of $CaSO_4 \cdot nH_2O$ products. Three repetitions were performed, and an average value was reported. After evaporation and formation had occurred completely, the product ($CaSO_4 \cdot nH_2O$) was kept in a desiccator for the sample characterization process.

2.2. Characterization

An XRF spectrometer (Bruker, Karlsruhe, Germany, SRS 3400) was employed to investigate the elemental compositions of the raw materials (hen and duck eggshell powders, $CaCO_3$) as well as the synthesized calcium sulfate samples ($CaSO_4 \cdot nH_2O$) using operation conditions of 100 mA current and 50 kV voltage. An XRD (Bruker, D8 Advance) diffractometer was employed to characterize the crystallographic characteristics of the sample (conditions: 40 mA and 40 kV). The diffraction database (powder diffraction file, PDF) generated by the International Centre for Diffraction Data (ICDD) [33] was used to confirm the experimental diffraction patterns of the sample. The diffraction was recorded from 5 to 60° (2θ angles) with a 0.01° increment and 1 s/step as the scan speed. An FTIR spectrometer (PerkinElmer, Waltham, MA, USA, Spectrum GX) was employed to record the infrared absorption spectra of the sample, and the recorded spectra were used for the identification of the functional groups (i.e., CO_3^{2-}, SO_4^{2-}, and H_2O) that existed in the sample structure. Each sample was first mixed with spectroscopic-grade potassium bromide powder and then pressed to form a small sample pellet for infrared measurement [34]. Infrared spectra of the samples were recorded at 4000–400 cm^{-1} (mid-infrared, MIR, region) using a resolution of 2 cm^{-1} and 64 scans. An SEM (Zeiss, Oberkochen, Germany, LEO VP1450) was used to observe the sample morphology after the gold coating technique.

3. Results and Discussion

3.1. Elemental Composition

The elemental compositions of the raw $CaCO_3$ materials (hen and duck eggshell powders) and their reacted products ($CaSO_4 \cdot nH_2O$) were measured by the XRF technique, and the results are listed in Table 1. The major elemental component of both hen and duck eggshell powders is CaO, and we recorded contents of 97.0 and 97.4 wt%, respectively. These confirmed the chemical presentation of $CaCO_3$ [23]. However, other compounds (mainly in oxide forms, as shown in Table 1) were also observed with total contents of 3.01 and 2.53 wt% for the hen and duck $CaCO_3$ samples, respectively. These experimental values are in agreement with the results reported in the literature. Hossain et al. [23] used the wavelength-dispersive XRF technique to evaluate the elemental composition of eggshells, and the results showed that CaO was the major component (97.0%). They also observed MgO (~1.08%), P_2O_5 (~0.457%), and Na_2O (~0.17%) as minor compounds. CuO is not present in hen eggshells but is present in duck eggshells, which may be due to hens' and ducks' different diets (with different mineral contents) in animal husbandry.

The $CaSO_4 \cdot nH_2O$ products synthesized from hen and duck eggshell powders were composed of two major elemental components: CaO (39.7 wt%) and sulfur trioxide (SO_3, 58.8 and 59.40 wt%). Other minor compounds in oxide forms were also observed, with total contents of 1.54 and 0.928 wt% for HES-$CaSO_4 \cdot nH_2O$ and DES-$CaSO_4 \cdot nH_2O$, respectively. As listed in Table 1, the raw $CaCO_3$ materials (HES and DES) powdered from hen and duck eggshells were found to have an insignificant difference in their CaO (97.00 and 97.40 wt%) contents. These raw $CaCO_3$ materials with the same content of CaO (39.70 wt%), after being reacted with the SO_4^{2-} source (H_2SO_4), were observed in both the HES-$CaSO_4 \cdot nH_2O$ and DES-$CaSO_4 \cdot nH_2O$ products. Although both products showed the same content of CaO, a slight difference in the SO_3 content (0.6 wt%) was observed, which might have arisen from Ca^{2+} sources that initially contained different SO_3 contents (0.644 and 1.08 wt% for hen and duck eggshells, respectively). The lowest content of minor components (0.928 wt%) indicated the highest purity of the DES-$CaSO_4 \cdot nH_2O$ product. Hence, it could be inferred

that the preparation of $CaSO_4 \cdot nH_2O$ by using duck eggshell waste as a renewable source provided the highest purity of the product. In addition, toxic metals, i.e., lead, arsenic, cadmium, and chromium, were not found in the hen and duck eggshell wastes (HES and DES), highlighting their green characteristics for use as eco-friendly and low-cost renewable sources for the production of value-added products like hydrated calcium sulfate ($CaSO_4 \cdot nH_2O$).

Table 1. Elemental composition of raw $CaCO_3$ materials (hen eggshell: HES; duck eggshell: DES) and $CaSO_4 \cdot nH_2O$ products derived from HES and DES (three repetitions were conducted, and average values are reported).

Elemental Composition		Elemental Contents/wt%			
		HES	DES	HES-$CaSO_4 \cdot nH_2O$	DES-$CaSO_4 \cdot nH_2O$
Calcium oxide	CaO	97.00	97.40	39.70	39.70
Sulfur trioxide	SO_3	0.64	1.08	58.80	59.40
Sodium oxide	Na_2O	0.21	0.17	0.10	0.07
Magnesium oxide	MgO	0.93	0.37	0.76	0.29
Aluminum oxide	Al_2O_3	0.13	0.04	0.06	0.02
Silicon dioxide	SiO_2	0.36	0.13	0.17	0.05
Phosphorus pentoxide	P_2O_5	0.51	0.62	0.34	0.40
Potassium oxide	K_2O	0.10	0.05	0.05	0.03
Ferric oxide	Fe_2O_3	0.07	0.034	0.03	0.03
Strontium oxide	SrO	0.06	0.01	0.02	0.03
Chlorine	Cl	0.02	0.02	–	–
Cupric oxide	CuO	–	0.01	–	–

3.2. Reaction Times and Product Yields

The "reaction time" was considered the time taken to dissolve eggshell $CaCO_3$ powders in H_2SO_4 solution completely, then generate a calcium sulfate (Ca^{2+}-SO_4^{2-}) salt solution, as demonstrated in Equation (1). Table 2 illustrates the reaction time recorded during the generation of salt solution.

Table 2. Reaction times and product yields of $CaSO_4 \cdot nH_2O$ derived from hen or duck eggshell powders and 50% w/w H_2SO_4 (three repetitions were conducted, and average values are reported).

Samples	Reaction Time/s	Product Yields/%
Hen-eggshell-derived $CaSO_4 \cdot nH_2O$	62	84.73
Duck-eggshell-derived $CaSO_4 \cdot nH_2O$	55	87.74

As described in Section 2.1, to achieve the complete chemical reaction, the molar ratio required between eggshell $CaCO_3$ powder and H_2SO_4 solution was 1:1, forming Ca^{2+}-SO_4^{2-}-H_2O solution. We observed that the temperature of the reaction increased, demonstrating that the dissolution process is an exothermic reaction. As can be seen in Table 2, there was an insignificant difference between the reaction times observed for the hen and duck eggshell systems; however, the results indicated that duck eggshell waste should be selected as the Ca^{2+} source used to rapidly prepare Ca^{2+}-SO_4^{2-} solution in a large-scale system.

As shown in Equations (1) and (2), the yields (Y_p/%) of $CaSO_4 \cdot nH_2O$ products prepared from eggshell $CaCO_3$ raw materials were computed by using Equation (3) [29]:

$$Y_P = \frac{wt_{ocs}}{wt_{tcs}} \times 100\% \quad (3)$$

where wt_{ocs} and wt_{tcs} (g) are the weights of $CaSO_4 \cdot nH_2O$ observed and in theory, respectively.

Table 2 lists the yields of $CaSO_4 \cdot nH_2O$ products synthesized from the two different eggshell wastes and 50% w/w H_2SO_4. The yields of the prepared $CaSO_4 \cdot nH_2O$ products derived from hen and duck eggshells are 84.73 and 87.74%, respectively. The product yields reported in this work are higher than that reported in a previous work (<80%) [29]. These results highlight that to achieve the highest $CaSO_4 \cdot nH_2O$ yield on a plant scale with a short reaction time, duck eggshell waste should be selected as the starting material for the $CaSO_4 \cdot nH_2O$ preparation. The reaction times of the gypsum products synthesized from the two kinds of eggshell wastes in this work are shorter than those reported in previous research (24 h) [23,24].

3.3. Vibrational Spectroscopy

The vibrational characteristics of the functional groups of the samples were observed and identified using an FTIR spectrometer, and the spectra of $CaCO_3$ and $CaSO_4 \cdot nH_2O$ in the MIR range (4000−400 cm^{-1}) are demonstrated in Figures 1 and 2, respectively. The functional group associated with the eggshell $CaCO_3$ samples is the carbonate (CO_3^{2-}) anion, whereas sulfate (SO_4^{2-}) and water (H_2O) are the functional groups of the $CaSO_4 \cdot nH_2O$ products. Therefore, the vibrational characteristics of the samples were characterized and mainly assigned based on the asymmetric stretching, symmetric stretching, and bending vibrational modes of CO_3^{2-}, SO_4^{2-}, and H_2O.

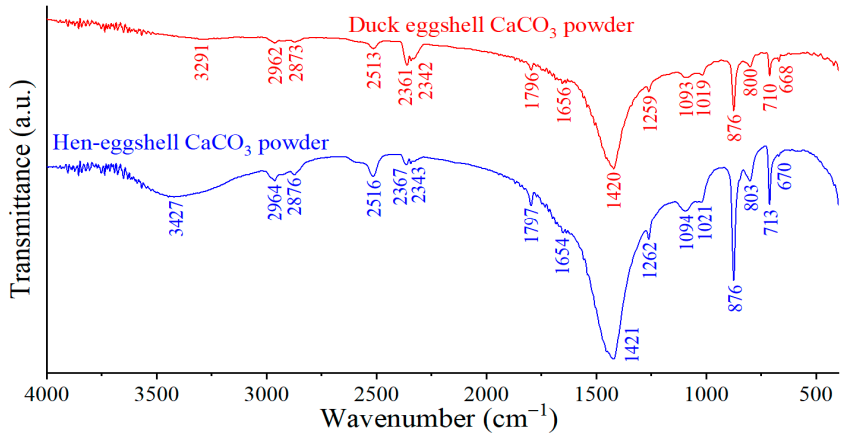

Figure 1. Infrared (IR) spectra of the hen- and duck-eggshell $CaCO_3$ powders in the wavenumber range of 4000−400 cm^{-1}.

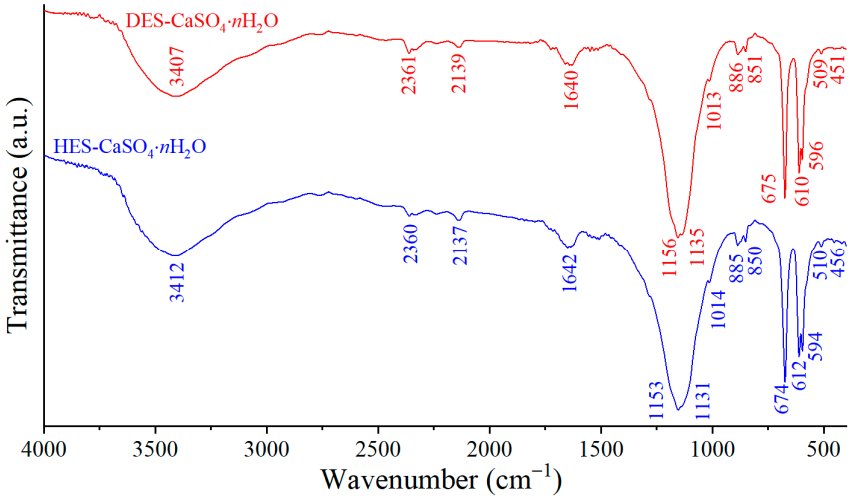

Figure 2. Infrared (IR) spectra of $CaSO_4 \cdot nH_2O$ products derived from hen and duck eggshell $CaCO_3$ raw materials: Hen-$CaSO_4 \cdot nH_2O$ and Duck-$CaSO_4 \cdot nH_2O$.

$CaCO_3$ can crystallize in three anhydrous polymorphs, e.g., calcite, aragonite, and vaterite, [35]; however, calcite is the most stable form under ambient conditions (room temperature and 1 atm) [36], while aragonite is slightly observed [37] and vaterite is formed under high specific conditions [38]. The FTIR spectroscopic technique was previously applied in the literature to quantify the vibrational modes of calcite and aragonite $CaCO_3$ polymorphs [37]. Therefore, the spectroscopic technique was selected in this work to identify the crystal structure (polymorph) of $CaCO_3$ milled from hen and duck eggshells, and the infrared spectra of $CaCO_3$ samples are demonstrated in Figure 1. The vibrational bands were considered based on the vibrational positions of trigonal planar CO_3^{2-}, which consists of four absorption modes: asymmetric (υ_3) and symmetric (υ_1) stretching modes between C and O atoms, and out-of-plane (υ_2) and in-plane (υ_4) bending modes between C and two O atoms. Another two vibrational characteristic combinations—between υ_1 and υ_3, and between υ_1 and υ_4—were also previously reported [37].

Calcite and aragonite $CaCO_3$ polymorphs show slightly different absorption positions overall, but various absorption positions between calcite and aragonite overlap [36,37]. Previously, three absorption positions of 670, 1021, and 1094 cm^{-1} of hen eggshell $CaCO_3$ powder or 668, 1019, and 1093 cm^{-1} of duck eggshell $CaCO_3$ powder were assigned as the vibrational characteristics of an aragonite $CaCO_3$ polymorph [36,37], whereas, in this study, other absorption positions were assigned as the vibrational characteristics of calcite $CaCO_3$. This revealed that both eggshell waste powders mainly contained the calcite $CaCO_3$ polymorph, with a very small aragonite $CaCO_3$ amount. The vibrational characteristics of the milled $CaCO_3$ samples are listed in Table 3.

Table 3. Vibrational characteristics and their absorption positions of the hen eggshell $CaCO_3$ (hen-$CaCO_3$) and duck eggshell $CaCO_3$ (duck-$CaCO_3$) powders.

Vibrational Characteristics	Positions/cm^{-1}	
	Hen-$CaCO_3$	**Duck-$CaCO_3$**
	CO_3^{2-}	
Asymmetric C−O stretching (υ_3)	1421, 1262	1420, 1259
Symmetric C−O stretching (υ_1)	1094, 1021	1093, 1019
O−C−O out-of-plane bending (υ_2)	876, 803	876, 800
O−C−O in-plane bending (υ_4)	713, 670	710, 668
$\upsilon 2 + \upsilon 3 + \upsilon 4$ combination	2964, 2876	2962, 2873
$\upsilon 1 + \upsilon 3$ combination	2516	2513
$\upsilon 1 + \upsilon 4$ combination	1797	1796
	H_2O	
Asymmetric (υ_3) and symmetric (υ_1) O−H stretching	3427	3291
H−O−H bending (υ_2)	1654	1656
	CO_2	
Asymmetric C-O stretching	2367, 2343	2361, 2342

Figure 2 shows the infrared spectra of the $CaSO_4 \cdot nH_2O$ products derived from hen and duck eggshell $CaCO_3$ raw materials. The vibrational modes (asymmetric stretching, symmetric stretching, and bending) of SO_4^{2-} and H_2O were mainly considered and assigned.

Takahashi et al. [39] carried out factor group analysis of gypsum ($CaSO_4 \cdot 2H_2O$) and reported that the symmetric stretching vibration (υ_1 (A_1, single mode, one component)) of the SO_4^{2-} ions belongs to the A_u symmetric species. The bending vibration (υ_2 (E, doubly degenerate mode, two components)) also belongs to A_u symmetry. Both the asymmetric stretching (υ_3 (F_2, triply degenerate mode, three components)) and bending (υ_4 (F2, triply degenerate mode, three components)) vibrations belong to two symmetric species: A_u

(one component) and B_u (two components). This previously obtained information was used for the assignment of the vibrational characteristics of the synthesized $CaSO_4 \cdot 2H_2O$. All observed vibrations of $CaSO_4 \cdot nH_2O$ products derived from hen and duck eggshell $CaCO_3$ powders, as listed in Table 4, were interpreted. Two vibrational positions at 510 and 456 cm^{-1} were assigned as the v_2 mode of SO_4^{2-} [39]. In addition, these two bands were also assigned as the vibrational modes (rocking, wagging, and twisting) of H_2O [40]. Three vibrational positions at 674, 612, and 594 cm^{-1} were assigned as the v_4 mode of SO_4^{2-}. This observation is in agreement with the vibrational characteristics of $CaSO_4 \cdot 2H_2O$ reported by Kayabaş and Yildirim [41]. The peak at 674 cm^{-1} is prominent, whereas the two peaks at 612 and 594 cm^{-1} are weaker. This phenomenon is in agreement with the results reported by Takahashi et al. [39]. The intensities of these three peaks exhibit remarkable polarization dependence, indicating that the direction of the transition moment of the 674 cm^{-1} peak is parallel, while the transition moments of the 612 and 594 cm^{-1} peaks are perpendicular to the *c*-axis. Three modes—v_1 (symmetric O−H stretching), v_2 (H−O−H bending), and v_3 (asymmetric O−H stretching)—of H_2O in $CaSO_4 \cdot 2H_2O$ crystals are in the A_u and B_u symmetry species. A peak at 3412 cm^{-1} is assigned as both the asymmetric (v_3) and symmetric (v_1) O−H stretching modes (belonging to B_u symmetry) of H_2O, whereas a peak at 1642 cm^{-1} is assigned as the H−O−H bending (v_2) mode of H_2O. All these observed vibrational bands are in agreement with results reported by Salvadori et al. [42] and Hossain et al. [23], which confirm the presence of SO_4^{2-} and H_2O. Other vibrational modes and their positions of SO_4^{2-} and H_2O, as well as CO_2 (adsorbed gas on the surface of the sample), are listed in Table 4.

Table 4. Vibrational characteristics and their absorption positions for $CaSO_4 \cdot nH_2O$ products derived from hen and duck eggshell $CaCO_3$ raw materials: hen-$CaSO_4 \cdot nH_2O$ and duck-$CaSO_4 \cdot nH_2O$.

Vibrational Characteristics	Positions/cm^{-1}	
	Hen-$CaSO_4 \cdot nH_2O$	**Duck-$CaSO_4 \cdot nH_2O$**
	SO_4^{2-}	
Asymmetric S−O stretching (v_3)	1153, 1131	1156, 1135
Symmetric S−O stretching (v_1)	1014	1013
$v_1 + v_3$ combination	2137	2139
O−S−O bending (v_4)	674, 612, 594	675, 610, 596
O−S−O bending (v_2)	510, 456	509, 451
	H_2O	
Asymmetric (v_3) and symmetric (v_1) O−H stretching	3412	3407
H−O−H bending (v_2)	1642	1640
Vibrations (rocking, wagging, twisting)	885, 850, 510, 456	886, 851, 509, 451
	CO_2	
Asymmetric C–O stretching	2360	2361, 2342

3.4. Crystallographic Characteristics

As described in the vibrational spectroscopic results, calcite and aragonite polymorphic crystals of $CaCO_3$ were observed. Therefore, another powerful technique, XRD, was used for the characterization of different $CaCO_3$ polymorphs [36,37]. The diffraction patterns (relationships between the XRD intensity and 2θ angle) of hen and duck eggshell waste powders are demonstrated in Figure 3a.

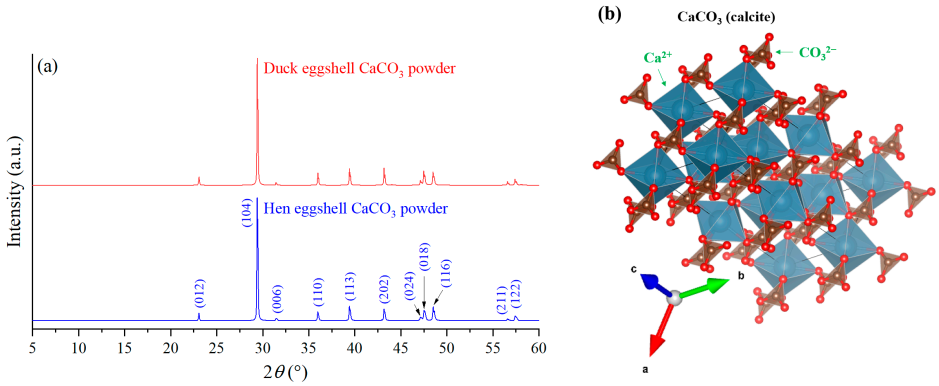

Figure 3. (**a**) X-ray diffraction (XRD) patterns of hen and duck eggshell waste $CaCO_3$ powders; (**b**) crystal structure of $CaCO_3$ in calcite polymorph, which consists of Ca^{2+} (CaO_6 octahedron) and CO_3^{2-} (trigonal planar) units.

Similar diffraction patterns between hen and duck eggshell waste powders were observed (Figure 3a), indicating that both materials (hen and duck eggshell powders) had the same crystallographic characteristics. All diffraction peaks were consistent with the standard diffraction data, PDF-ICDD #47-1743 [43], revealing that only the calcite $CaCO_3$ polymorph was observed, which is the natural polymorph of $CaCO_3$ present in the eggshell [44]. No diffraction peak of the aragonite $CaCO_3$ polymorph was observed. This result might have been since there was a very small amount of aragonite $CaCO_3$, which was not observed in the XRD technique [44]. Smooth diffraction baselines with high diffraction intensity peaks, as exhibited in Figure 3a, indicated the high crystallinity of $CaCO_3$ powders obtained from both hen and duck eggshells. Figure 3b shows the crystal structure of $CaCO_3$ in the calcite polymorph [15]. The lattice parameters *a* and *c* of calcite $CaCO_3$ are 4.9896 and 17.0610 Å, with a cell volume of 367.8537 $Å^3$ [37]. The crystallite sizes (S_c) of the samples were calculated by using the main diffraction (*hkl* lattice plane: 104; 2θ angles: 29.40° and 29.41° for hen and duck eggshell $CaCO_3$ samples) through the Scherrer equation (Equation (4)) [45].

$$S_c = \frac{0.89\lambda}{\beta\, cos\theta} \quad (4)$$

where λ is the X-ray wavelength (1.5406 Å), β is the full width at half-maximum (FWHM) value of the selected XRD diffraction peak, and θ is the angle of the selected diffraction peak.

The calculated crystallite sizes for the (104) calcite-lattice plane are listed in Table 5 for hen and duck eggshell waste $CaCO_3$ powders, respectively.

Table 5. Crystallite sizes (S_c) of the prepared samples calculated from lattice planes (*hkl*), full width at half-maximum (FWHM, β), and diffraction peaks (2θ, θ).

Samples	*hkl* Planes	β/°	2θ/°	θ/°	S_c/nm
Hen-$CaCO_3$	(104)	0.13763	29.40	14.700	18.67
Duck-$CaCO_3$		0.12451	29.41	14.705	20.48
Hen-CaO	(220)	0.18188	37.66	18.830	7.54
Duck-CaO		0.17062	37.62	18.810	8.04
Hen-$CaSO_4{\cdot}2H_2O$	(020)	0.07774	11.67	5.835	19.57
Duck-$CaSO_4{\cdot}2H_2O$		0.07863	11.68	5.840	19.30
Hen-$CaSO_4$	(200)	0.11701	25.42	12.710	11.84
Duck-$CaSO_4$		0.12425	25.47	12.735	11.19

Other crystallographic data (observed 2θ positions, diffraction intensities, the standard *d*-spacing values, and *hkl* lattice planes [46]) of hen and duck eggshell $CaCO_3$ powders are listed in Table 6. These obtained data—specifically the higher intensities of all diffraction peaks, except for the (116) lattice plane—indicated that good crystallinity was obtained for the duck eggshell $CaCO_3$ sample.

Table 6. Crystallographic data of hen and duck eggshell $CaCO_3$ powders.

2θ/°		Diffraction Intensity/a.u.		*d*-Spacing/Å	*hkl* Planes/-
Hen-$CaCO_3$	Duck-$CaCO_3$	Hen-$CaCO_3$	Duck-$CaCO_3$		
23.40	23.08	8587	9654	3.8556	(012)
29.40	29.41	143,135	147,710	3.0364	(104)
31.49	31.43	2717	3090	2.8448	(006)
35.97	35.99	10,136	14,082	2.4951	(110)
39.42	39.42	16,789	19,140	2.2851	(113)
43.17	43.17	13,453	20,007	2.0948	(202)
47.13	47.12	3795	5420	1.9278	(024)
47.52	47.49	12,098	16,631	1.9131	(018)
48.53	48.50	16,047	15,125	1.8758	(116)
56.58	56.59	1801	4286	1.6260	(211)
57.44	57.40	5223	6935	1.6043	(122)

The diffraction patterns of the products obtained from the calcination process of raw hen and duck eggshell waste powders, as demonstrated in Figure 4a, showed three crystalline phases, consisting of CaO (lime), calcium hydroxide ($Ca(OH)_2$, portlandite), and calcite $CaCO_3$. Diffraction peaks at 32.47°, 37.62°, and 54.10° (Figure 4a) were assigned to the (111), (200), and (220) lattice planes of CaO based on PDF-ICDD #74-1226 [47], and Figure 4b shows the crystal structure of CaO [48]. Conventionally, a small fraction of CaO material can adsorb atmospheric H_2O, resulting in the formation of $Ca(OH)_2$ crystals due to the exposure of CaO to the air. The presence of $Ca(OH)_2$ was confirmed by PDF-ICDD #01-1079 with 2θ results of 18.26, 34.23, and 47.37° for the (001), (101), and (102) lattice planes of $Ca(OH)_2$ [49]. A diffraction peak at 29.66° (for both hen-and duck $CaCO_3$) was observed, which is the highest diffraction intensity of calcite $CaCO_3$, corresponding to the (104) lattice plane [37]. The crystallite sizes of CaO samples calculated from the Scherrer equation are listed in Table 5.

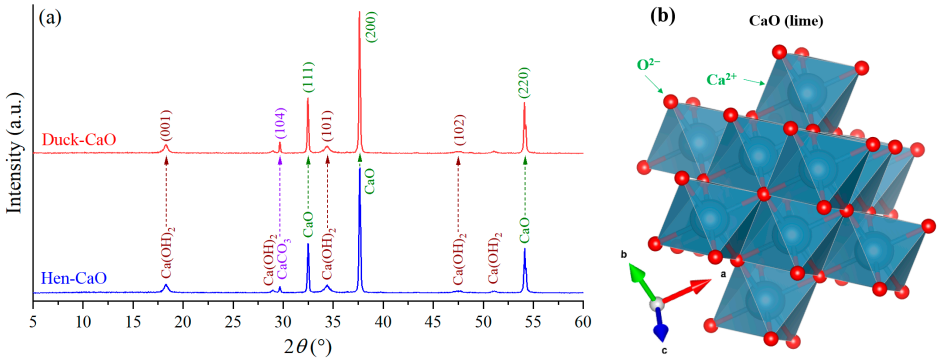

Figure 4. (**a**) X-ray diffraction (XRD) patterns of calcined product (CaO, lime) obtained from the calcination process (900 °C, 2 h) of hen and duck eggshell waste ($CaCO_3$) powders; (**b**) crystal structure of CaO, which consists of Ca^{2+} and O^{2-} units (CaO_6 octahedron).

The experimental diffraction pattern and the crystal structure [50] of the synthesized $CaSO_4 \cdot nH_2O$ product are demonstrated in Figure 5a,b, respectively. All diffraction peaks (Figure 5a) observed for the synthesized products were consistent with the standard

diffraction of PDF-ICDD #33-0311, demonstrating the diffraction characteristics of gypsum ($CaSO_4 \cdot 2H_2O$) [23,51].

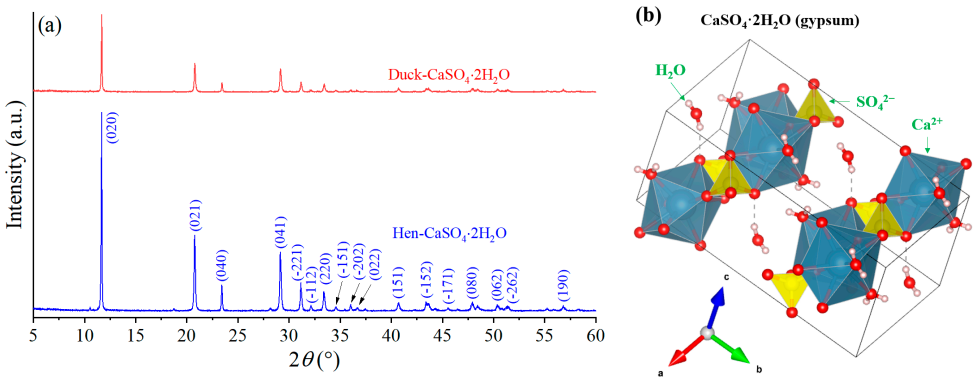

Figure 5. (**a**) X-ray diffraction (XRD) patterns of $CaSO_4 \cdot 2H_2O$ (gypsum) prepared from the reaction between hen or duck eggshell waste ($CaCO_3$) powder and H_2SO_4; (**b**) crystal structure of $CaSO_4 \cdot 2H_2O$, which consists of Ca^{2+} (CaO_8 polyhedron), SO_4^{2-} (tetrahedron), and H_2O units.

Given the similarity of the diffraction patterns of the hen and duck $CaSO_4 \cdot 2H_2O$ products, we surmised that both prepared products had the same structural and chemical characteristics, which were those of gypsum ($CaSO_4 \cdot 2H_2O$). The characteristic peaks of other phases were not observed in the diffraction patterns, indicating that $CaSO_4 \cdot 2H_2O$ might be formed as a single phase or that other phases with small amounts were not observed by the XRD technique. The observed 2θ positions, diffraction intensities, standard *d*-spacing values, and *hkl* lattice planes of hen- and duck-eggshell-derived $CaSO_4 \cdot 2H_2O$ samples are listed in Table 7.

Table 7. Crystallographic data of $CaSO_4 \cdot 2H_2O$ samples derived from hen and eggshell $CaCO_3$ raw materials.

2θ/°		Diffraction Intensity/a.u.		*d*-Spacing/Å	*hkl* Planes/-
Hen-$CaSO_4 \cdot 2H_2O$	Duck-$CaSO_4 \cdot 2H_2O$	Hen-$CaSO_4 \cdot 2H_2O$	Duck-$CaSO_4 \cdot 2H_2O$		
11.67	11.68	2699	1051	7.6000	(020)
20.79	20.78	1030	394	4.2811	(021)
23.41	23.43	360	129	3.8000	(040)
29.14	29.17	804	316	3.0642	(041)
31.15	31.17	390	139	2.8730	(−221)
32.13	32.19	84	32	2.7875	(−112)
33.41	33.45	279	114	2.6828	(220)
34.57	34.64	66	30	2.5964	(−151)
36.02	36.11	97	33	2.4957	(−202)
36.67	36.60	55	34	2.4521	(022)
40.69	40.69	121	59	2.2174	(151)
43.39	43.64	136	62	2.0860	(−152)
45.54	45.56	51	29	1.9912	(−171)
47.94	47.96	132	53	1.8985	(080)
50.40	50.35	94	47	1.8113	(062)
55.24	55.20	47	24	1.6643	(−262)
56.80	56.80	85	48	1.6207	(190)

The crystallite sizes calculated by using Scherrer's equation for the hen and duck $CaSO_4 \cdot 2H_2O$ samples are listed in Table 5. Pinto et al. [52] synthesized pure $CaSO_4 \cdot 2H_2O$ by using $CaCl_2$ and Na_2SO_4 as the Ca^{2+} and SO_4^{2-} sources, respectively. The lattice

parameters of $CaSO_4 \cdot 2H_2O$ were then calculated and found to comprise *a*, *b*, and *c* values of 5.675, 15.214, and 6.284 Å, respectively. $CaSO_4 \cdot 2H_2O$ crystallizes in a monoclinic crystal system with the space group *C*2/*c* (#15) [23]. The relative intensity (*Ri*), an important parameter, was also calculated in this work from the experimental XRD data. The *Ri* for the highest diffraction intensity ((020) plane) was calculated from the other three strong lattice planes—(021), (040), and (041)—using Equation (5) [23]:

$$R_i = \frac{Int_{020}}{Int_{021} + Int_{040} + Int_{041}} \quad (5)$$

where $Int_{(020)}$, $Int_{(021)}$, $Int_{(040)}$, and $Int_{(041)}$ are the intensities of the diffraction peaks of the (020), (021), (040), and (041) lattice planes, respectively.

The *Ri* values of the hen and duck $CaSO_4 \cdot 2H_2O$ samples were 1.23 and 1.25, respectively. In order to compare the *Ri* values, the *Ri* of the diffraction database (PDF-ICDD #33-0311) was also calculated for the same lattice planes and found to be 0.52. The preferential growth (*Pg*) parameter of the (020) plane was then calculated using Equation (6) [23]:

$$P_g = \frac{Ri_{ss} - Ri_{sd}}{Ri_{sd}} \quad (6)$$

where Ri_{ss} and Ri_{sd} are the relative intensities of the synthesized sample ($CaSO_4 \cdot 2H_2O$) and the standard data (PDF-ICDD #33-0311, *Ri* = 0.52), respectively.

The *Pg* values for the synthesized hen and duck $CaSO_4 \cdot 2H_2O$ samples were calculated and found to be 4.54 and 4.62, respectively. The positive values we obtained suggested that the growth along the (020) lattice plane was stable and favorable, indicating good crystal stability [23].

Figure 6a demonstrates the diffraction patterns of products obtained from the calcination step (900 °C, 2 h) of $CaSO_4 \cdot 2H_2O$. All diffraction peaks show the structural characteristics of the anhydrite ($CaSO_4$) phase. As described in the Section 1, two polymorphs of $CaSO_4$ were reported, β-$CaSO_4$ and γ-$CaSO_4$, which are the stable and metastable forms, respectively [16]. The hydration rate of the γ polymorph ($CaSO_4$(s) + nH_2O(g) $\rightarrow$ $CaSO_4 \cdot nH_2O$(s)) is greater than that of the β polymorph; consequently, if the γ form comes in contact with atmospheric water, its rehydration process will occur, preventing the formation of the γ form [53].

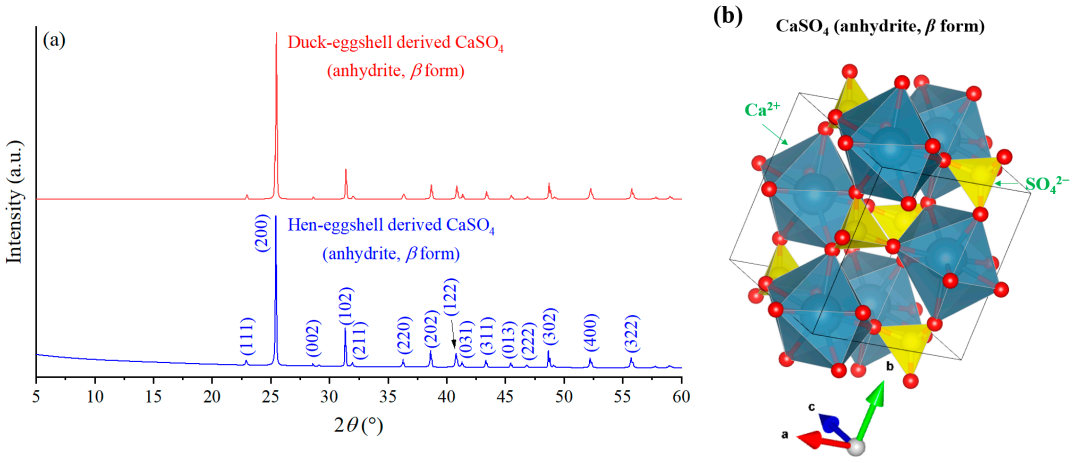

Figure 6. (**a**) X-ray diffraction (XRD) patterns of $CaSO_4$ (anhydrite) obtained from the calcination process (900 °C, 2 h) of $CaSO_4 \cdot 2H_2O$; (**b**) crystal structure of β-$CaSO_4$, which consists of Ca^{2+} (CaO_8 polyhedron) and SO_4^{2-} (tetrahedron) units.

All diffraction peaks of both $CaSO_4$ samples, obtained from hen- and duck-eggshell-derived $CaSO_4 \cdot 2H_2O$, were consistent with PDF-ICDD #72-0916. This standard diffraction

confirmed that the product of the calcination process of $CaSO_4 \cdot 2H_2O$ is the orthorhombic $CaSO_4$ phase with β polymorphic crystals. The crystal structure of β-$CaSO_4$ [54] is shown in Figure 6b. The crystallite sizes of β-$CaSO_4$ samples calculated from the Scherrer equation are listed in Table 5.

3.5. Morphological Characteristics

The morphological characteristics of hen and duck eggshell $CaCO_3$ raw materials and their reaction products ($CaSO_4 \cdot 2H_2O$) were imaged with a magnification of 15 k*x*, and the resulting micrographs of the samples are presented in Figure 7. The micrographs of the $CaCO_3$ particles obtained from the milling process of raw hen and duck eggshell powders present an agglomeration of $CaCO_3$ particles, causing different particle sizes. These different particle sizes were obtained since milling is a mechanical process, commonly employed for material size reduction through centrifugal forces [55]. During the milling process, some fractions of eggshells were milled completely, resulting in small powdered particles, whereas other fractions were not milled completely, resulting in large powdered particles. In addition, during the rotation process, small particles were randomly moved and located on the surface of large particles.

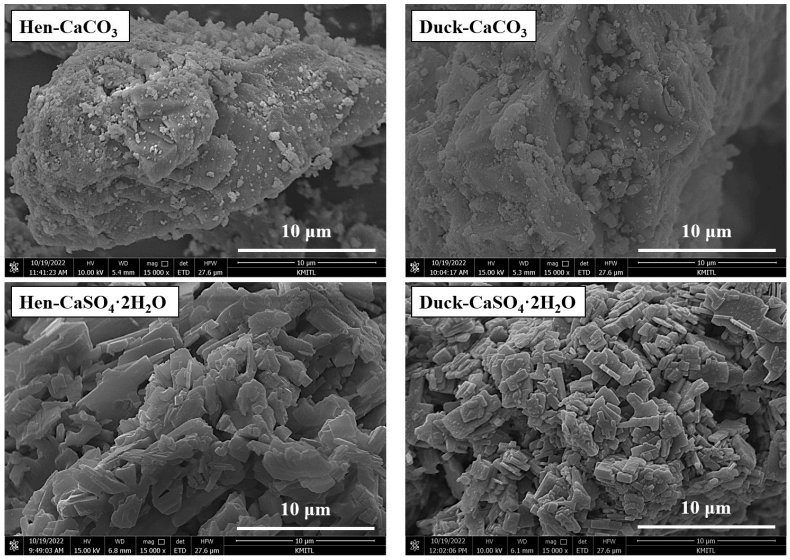

Figure 7. Scanning electron microscopic (SEM) images of $CaCO_3$ powders obtained from the milling process of hen and duck eggshell wastes, and the products ($CaSO_4 \cdot 2H_2O$, gypsum) prepared from the reaction between hen or duck eggshell waste powder and H_2SO_4.

The micrographs of the $CaSO_4 \cdot 2H_2O$ samples synthesized from the reaction between hen or duck eggshell $CaCO_3$ raw material and H_2SO_4, as demonstrated in Figure 7, show plate-like particles. This finding is not consistent with the results reported in the literature. Mbogoro et al. [56] used commercial $CaCl_2 \cdot 2H_2O$ and Na_2SO_4 as Ca^{2+} and SO_4^{2-} sources, respectively, to form $CaSO_4 \cdot 2H_2O$ crystals. The same concentration of Ca^{2+} and SO_4^{2-} salts of 0.56 mol/L was prepared as stock solutions and then those were employed to prepare growth solutions with five different Ca^{2+}:SO_4^{2-} free-ion ratios of 2.5:18.8, 3.4:13.7, 6.9:6.8, 13.6:3.4, and 17.8:2.5, corresponding to the ionic ratios (r) of 0.13, 0.25, 1.01, 4.00, and 7.12, respectively. At low ionic ratios ($r < 1$, SO_4^{2-}-rich solutions), plate-like $CaSO_4 \cdot 2H_2O$ crystals were observed, whereas needle-like crystals were observed at an equal stoichiometry ($r = 1$) and at high ionic ratios ($r < 1$, Ca^{2+}-rich solutions) [56]. Moreover, Madeja et al. [57] also used commercial $CaCl_2 \cdot 2H_2O$ and Na_2SO_4 solutions to prepare $CaSO_4 \cdot 2H_2O$ using titration precipitation and then investigated the influences of various additives (small molecules, homo- and co-polymers) on the morphological characteristics of $CaSO_4 \cdot 2H_2O$. Among the additives, a co-polymer of vinylpyrrolidone (PVP) and acrylic acid (PAA) acted as an important modifier for gypsum development. $CaSO_4 \cdot 2H_2O$ particles with tilted stacking

edges and pseudo-hexagonal plates were obtained [57]. In this work, irregular plate-like $CaSO_4 \cdot 2H_2O$ particles were observed by using an ionic ratio between Ca^{2+} (hen or duck eggshell $CaCO_3$) and SO_4^{2-} (H_2SO_4) of 1 (as described in "*Materials and their Synthesis*", Equations (1) and (2)) without an additive addition step. These results demonstrate that different formation conditions cause different morphological characteristics [56,57].

4. Conclusions

Gypsum ($CaSO_4 \cdot 2H_2O$) products were synthesized successfully using two kinds of eggshells (hen and duck) with a short time period and easy process, generating low-cost products. The experimental and standard diffraction patterns confirmed that the value-added product from the eggshell waste powders is $CaSO_4 \cdot 2H_2O$ (gypsum). When $CaSO_4 \cdot 2H_2O$ is thermally treated, it can completely dehydrate to form $CaSO_4$ (anhydrite, β polymorph). The diffraction patterns also indicated that the sample phase will change from a monoclinic ($CaSO_4 \cdot 2H_2O$) to an orthorhombic ($CaSO_4$) crystal structure. The morphological characteristics of $CaCO_3$ show an irregular shape with different agglomeration particle sizes, whereas plate-like particles were observed for $CaSO_4 \cdot 2H_2O$. The crystallite sizes calculated from the diffraction peak with the highest intensity for $CaCO_3$, CaO, $CaSO_4 \cdot 2H_2O$, and $CaSO_4$ were 18−21, 7−8, 19−20, and 11−12 nm, respectively.

This article has reported an easy and low-cost method with no environmental effect, which may be applied to produce cheap $CaSO_4 \cdot 2H_2O$ products to be used in the agroindustry, forming part of zero-waste sustainability efforts.

Author Contributions: C.S. and W.B.: investigation, experiment, data curation, writing—original draft, review and editing. P.P. and S.S.: data curation, writing—review and editing. B.B. and N.L.: conceptualization, investigation, writing—review and editing, supervision. P.R.: conceptualization, data curation, writing—review and editing. All authors have read and agreed to the published version of the manuscript.

Funding: This work is a result of the project entitled "Conversion of shell/eggshell biowastes for sustainable environmental remediation" (Grant No. RE-KRIS/FF67/030) of King Mongkut's Institute of Technology Ladkrabang (KMITL), which has received funding support from the NSRE.

Data Availability Statement: All data that support the findings of this study are available from the corresponding author upon reasonable request.

Acknowledgments: The authors would like to thank the Scientific Instruments Center KMITL for supporting the TGA, FTIR, XRD, and SEM techniques.

Conflicts of Interest: The authors declare no conflicts of interest.

References

1. Aranda, M.A.; Artioli, I.; Bier, T.; Àngeles, G.; Freyer, D.; Kaden, R.; Lothenbach, B.; Pritzel, C.; Raab, B.; Stöber, S. *Cementitious Materials: Composition, Properties, Application*; Walter de Gruyter GmbH & Co KG: Berlin/Heidelberg, Germany, 2017.
2. Kumar, Y.; Nalini, K.; Menon, J.; Patro, D.K.; Banerji, B. Calcium sulfate as bone graft substitute in the treatment of osseous bone defects, a prospective study. *J. Clin. Diagn. Res.* **2013**, *7*, 2926–2928. [CrossRef] [PubMed]
3. Mohammed, A.A.; Elsherbini, A.M.; Ibrahim, F.M.; El-Meadawy, S.M.; Youssef, J.M. Biological effect of the nanocrystalline calcium sulfate bone graft in the periodontal regeneration. *J. Oral Biol. Craniofacial Res.* **2021**, *11*, 47–52. [CrossRef] [PubMed]
4. Mukherji, A. Management of periradicular lesion using calcium sulfate graft: An unique case report. *CHRISMED J. Health Res.* **2017**, *4*, 268. [CrossRef]
5. Subramaniam, S.; Fang, Y.-H.; Sivasubramanian, S.; Lin, F.-H.; Lin, C. Hydroxyapatite-calcium sulfate-hyaluronic acid composite encapsulated with collagenase as bone substitute for alveolar bone regeneration. *Biomaterials* **2016**, *74*, 99–108. [CrossRef]
6. Guarnieri, R.; Bovi, M. Maxillary sinus augmentation using prehardened calcium sulfate: A case report. *Int. J. Periodont. Rest.* **2002**, *22*, 503–508.
7. Murariu, M.; Da Silva Ferreira, A.; Bonnaud, L.; Dubois, P. Calcium sulfate as high-performance filler for polylactide (PLA) or how to recycle gypsum as by-product of lactic acid fermentation process. *Compos. Interfaces* **2009**, *16*, 65–84. [CrossRef]
8. Wang, J.; Pan, X.; Xue, Y.; Cang, S. Studies on the application properties of calcium sulfate whisker in silicone rubber composites. *J. Elastomers Plast.* **2012**, *44*, 55–66. [CrossRef]
9. Al-Hadhrami, L.M.; Quddus, A.; Al-Otaibi, D.A. Calcium sulfate scale deposition on coated carbon steel and titanium. *Desalination Water Treat.* **2013**, *51*, 2521–2528. [CrossRef]

10. Burfield, D.R. Desiccant efficiency in solvent and reagent drying. 9. A reassessment of calcium sulfate as a drying agent. *J. Org. Chem.* **1984**, *49*, 3852–3854. [CrossRef]
11. Wenjing, L.; Yue, Z.; Cen, Z.; Di, C.; Chaogeng, X. Influence of calcium sulfate incorporated with gluconolactone coagulant on the quality of whole soybean flour tofu. *Food Chem. X* **2022**, *17*, 100527.
12. Zuhaimi, N.A.S.; Indran, V.P.; Deraman, M.A.; Mudrikah, N.F.; Maniam, G.P.; Taufiq-Yap, Y.H.; Rahim, M.H.A. Reusable gypsum based catalyst for synthesis of glycerol carbonate from glycerol and urea. *Appl. Catal. A Gen.* **2015**, *502*, 312–319. [CrossRef]
13. Chakawa, D.; Nkala, M.; Hlabangana, N.; Muzenda, E. The use of calcium sulphate dihydrate ($CaSO_4 \cdot 2H_2O$) as a bleaching agent for crude soya bean vegetable oil. *Procedia Manuf.* **2019**, *35*, 802–807. [CrossRef]
14. Yin, S.; Yang, L. α or β?-hemihydrates transformed from dihydrate calcium sulfate in a salt-mediated glycerol–water solution. *J. Cryst. Growth.* **2020**, *550*, 125885. [CrossRef]
15. Ishizawa, N.; Setoguchi, H.; Yanagisawa, K. Structural evolution of calcite at high temperatures: Phase V unveiled. *Sci. Rep.* **2013**, *3*, 2832. [CrossRef] [PubMed]
16. Schmid, T.; Jungnickel, R.; Dariz, P. Insights into the $CaSO_4$–H_2O system: A Raman-spectroscopic study. *Minerals* **2020**, *10*, 115. [CrossRef]
17. Freyer, D.; Voigt, W. Crystallization and phase stability of $CaSO_4$ and $CaSO_4$–based salts. *Monatshefte Chemie* **2003**, *134*, 693–719. [CrossRef]
18. Unjan, W.; Tangboriboon, N. Bio-calcium sulfate preparation from duck eggshell via chemical reaction process. *Int. J. Curr. Adv. Res.* **2017**, *6*, 2454–2459. [CrossRef]
19. Wang, Y.; Mao, X.; Chen, C.; Wang, W.; Dang, W. Effect of sulfuric acid concentration on morphology of calcium sulfate hemihydrate crystals. *Mater. Res. Express.* **2020**, *7*, 105501. [CrossRef]
20. Bakshi, P.; Pappu, A.; Bharti, D.K. Transformation of flue gas desulfurization (FGD) gypsum to β-$CaSO_4 \cdot 0.5H_2O$ whiskers using facile water treatment. *Mater. Lett.* **2022**, *308*, 131177. [CrossRef]
21. Kong, B.; Yu, J.; Savino, K.; Zhu, Y.; Guan, B. Synthesis of α-calcium sulfate hemihydrate submicron-rods in water/n-hexanol/CTAB reverse microemulsion. *Colloids Surf. A Physicochem. Eng. Asp.* **2012**, *409*, 88–93. [CrossRef]
22. Van Driessche, A.; Stawski, T.; Kellermeier, M. Calcium sulfate precipitation pathways in natural and engineered environments. *Chem. Geol.* **2019**, *530*, 119274. [CrossRef]
23. Hossain, M.S.; Shaikh, M.A.A.; Ahmed, S. Synthesis of Gypsum fertilizer from waste eggshells for sustainable environment. *Mater. Adv.* **2023**, *4*, 240–247. [CrossRef]
24. Hossain, M.S.; Ahmed, S. Synthesis of nano-crystallite gypsum and bassanite from waste *Pila globose* shells: Crystallographic Characterization. *RSC Adv.* **2022**, *12*, 25096–25105. [CrossRef]
25. Lee, W.-D.; Kothari, D.; Niu, K.-M.; Lim, J.-M.; Park, D.-H.; Ko, J.; Eom, K.; Kim, S.-K. Superiority of coarse eggshell as a calcium source over limestone, cockle shell, oyster shell, and fine eggshell in old laying hens. *Sci. Rep.* **2021**, *11*, 13225. [CrossRef]
26. Maslyk, M.; Dallos, Z.; Koziol, M.; Seiffert, S.; Hieke, T.; Petrović, K.; Kolb, U.; Mondeshki, M.; Tremel, W. A Fast and Sustainable Route to Bassanite Nanocrystals from Gypsum. *Adv. Funct. Mater.* **2022**, *32*, 2111852. [CrossRef]
27. Kamarou, M.; Natalia Korob, N.; Romanovski, V. Structurally controlled synthesis of synthetic gypsum derived from industrial wastes: Sustainable approach. *J. Chem. Technol. Biotechnol.* **2021**, *96*, 3134–3141. [CrossRef]
28. Kamarou, M.; Kuzmenkov, M.; Korob, N.; Kwapinski, W.; Romanovski, V. Structurally controlled synthesis of calcium sulphate dihydrate from industrial wastes of spent sulphuric acid and limestone. *Environ. Technol. Innov.* **2020**, *17*, 100582. [CrossRef]
29. Kumar, A.; Sharma, S.; Sharma, A.K. Synthesis of Gypsum Utilizing Waste Eggshell. *Int. J. Sci. Res. Dev.* **2021**, *9*, 305–309.
30. Umesh, M.; Choudhury, D.D.; Shanmugam, S.; Ganesan, S.; Alsehli, M.; Elfasakhany, A.; Pugazhendhi, A. Eggshells biowaste for hydroxyapatite green synthesis using extract piper betel leaf-evaluation of antibacterial and antibiofilm activity. *Environ. Res.* **2021**, *200*, 111493. [CrossRef]
31. Laohavisuti, N.; Boonchom, B.; Boonmee, W.; Chaiseeda, K.; Seesanong, S. Simple recycling of biowaste eggshells to various calcium phosphates for specific industries. *Sci. Rep.* **2021**, *11*, 15143. [CrossRef]
32. Wong-Ng, W.; McMurdie, H.; Hubbard, C.; Mighell, A.D. JCPDS-ICDD research associateship (cooperative program with NBS/NIST). *J. Res. Natl. Inst. Stand. Technol.* **2001**, *106*, 1013–1028. [CrossRef]
33. Sronsri, C.; Boonchom, B. Synthesis, characterization, vibrational spectroscopy, and factor group analysis of partially metal-doped phosphate materials. *Spectrochim. Acta A Mol. Biomol. Spectrosc.* **2018**, *194*, 230–240. [CrossRef]
34. Morse, J.W.; Arvidson, R.S.; Lüttge, A. Calcium carbonate formation and dissolution. *Chem. Rev.* **2007**, *107*, 342–381. [CrossRef]
35. Sronsri, C.; Sittipol, W.; U-yen, K. Performance of CaO catalyst prepared from magnetic-derived $CaCO_3$ for biodiesel production. *Fuel* **2021**, *304*, 121419. [CrossRef]
36. Sronsri, C.; U-yen, K.; Sittipol, W. Quantitative analysis of calcium carbonate formation in magnetized water. *Mater. Chem. Phys.* **2020**, *245*, 122735. [CrossRef]
37. Nahi, O.; Kulak, A.N.; Zhang, S.; He, X.; Aslam, Z.; Ilett, M.A.; Ford, I.J.; Darkins, R.; Meldrum, F.C. Polyamines promote aragonite nucleation and generate biomimetic structures. *Adv. Sci.* **2022**, *10*, 2203759. [CrossRef]
38. Takahashi, H.; Maehara, I.; Kaneko, N. Infrared reflection spectra of gypsum. *Spectrochim. Acta A Mol. Biomol. Spectrosc.* **1983**, *39*, 449–455. [CrossRef]
39. Cygan, R.T.; Daemen, L.L.; Ilgen, A.G.; Krumhansl, J.L.; Nenoff, T.M. Inelastic neutron scattering and molecular simulation of the dynamics of interlayer water in smectite clay minerals. *J. Phys. Chem. C* **2015**, *119*, 28005–28019. [CrossRef]

40. Kayabaş, A.; Yildirim, E. New approaches with ATR-FTIR, SEM, and contact angle measurements in the adaptation to extreme conditions of some endemic *Gypsophila* L. taxa growing in gypsum habitats. *Spectrochim. Acta A Mol. Biomol. Spectrosc.* **2022**, *270*, 120843. [CrossRef]
41. Salvadori, B.; Errico, V.; Mauro, M.; Melnik, E.; Dei, L. Evaluation of gypsum and calcium oxalates in deteriorated mural paintings by quantitative FTIR spectroscopy. *Spectrosc. Lett.* **2003**, *36*, 501–513. [CrossRef]
42. Render, D.; Samuel, T.; King, H.; Vig, M.; Jeelani, S.; Babu, R.J.; Rangari, V. Biomaterial-derived calcium carbonate nanoparticles for enteric drug delivery. *J. Nanomater.* **2016**, *2016*, 3170248. [CrossRef]
43. Gautron, J.; Stapane, L.; Le Roy, N.; Nys, Y.; Rodriguez-Navarro, A.; Hincke, M. Avian eggshell biomineralization: An update on its structure, mineralogy and protein tool kit. *BMC Mol. Cell Biol.* **2021**, *22*, 11. [CrossRef]
44. Monshi, A.; Foroughi, M.R.; Monshi, M.R. Modified Scherrer equation to estimate more accurately nano-crystallite size using XRD. *World J. Nano Sci. Eng.* **2012**, *2*, 154–160. [CrossRef]
45. Sitepu, H. Texture and structural refinement using neutron diffraction data from molybdite (MoO_3) and calcite ($CaCO_3$) powders and a Ni-rich $Ni_{50.7}Ti_{49.30}$ alloy. *Powder Diffr.* **2009**, *24*, 315–326. [CrossRef]
46. Liu, J.; Liu, M.; Chen, S.; Wang, B.; Chen, J.; Yang, D.-P.; Zhang, S.; Du, W. Conversion of Au(III)-polluted waste eggshell into functional CaO/Au nanocatalyst for biodiesel production. *Green Energy Environ.* **2022**, *7*, 352–359. [CrossRef]
47. Fiquet, G.; Richet, P.; Montagnac, G. High-temperature thermal expansion of lime, periclase, corundum and spinel. *Phys. Chem. Miner.* **1999**, *27*, 103–111. [CrossRef]
48. Yan, F.; Jiang, J.; Zhao, M.; Tian, S.; Li, K.; Li, T. A green and scalable synthesis of highly stable Ca-based sorbents for CO_2 capture. *J. Mater. Chem. A* **2015**, *3*, 7966–7973. [CrossRef]
49. Comodi, P.; Nazzareni, S.; Zanazzi, P.F.; Speziale, S. High-pressure behavior of gypsum: A single-crystal X-ray study. *Am. Miner.* **2008**, *93*, 1530–1537. [CrossRef]
50. Chen, Q.; Jiang, G.; Jia, C.; Wang, H.; Guan, B. A facile method to control the structure and morphology of α-calcium sulfate hemihydrate. *CrystEngComm* **2015**, *17*, 8549–8554. [CrossRef]
51. Pinto, A.J.; Carneiro, J.; Katsikopoulos, D.; Jiménez, A.; Prieto, M. The link between brushite and gypsum: Miscibility, dehydration, and crystallochemical behavior in the $CaHPO_4{\cdot}2H_2O$–$CaSO_4{\cdot}2H_2O$ system. *Cryst. Growth Des.* **2012**, *12*, 445–455. [CrossRef]
52. Christensen, A.N.; Olesen, M.; Cerenius, Y.; Jensen, T.R. Formation and transformation of five different phases in the $CaSO_4-H_2O$ system: Crystal structure of the subhydrate β-$CaSO_4{\cdot}0.5H_2O$ and soluble anhydrite $CaSO_4$. *Chem. Mater.* **2008**, *20*, 2124–2132. [CrossRef]
53. Antao, S.M. Crystal-structure analysis of four mineral samples of anhydrite, $CaSO_4$, using synchrotron high-resolution powder X-ray diffraction data. *Powder Diffr.* **2011**, *26*, 326–330. [CrossRef]
54. Borhan, M.Z.; Ahmad, R.; Rusop, M.; Abdullah, S. Optimization of ball milling parameters to produce *Centella asiatica* herbal nanopowders. *J. Nanostructure Chem.* **2013**, *3*, 79. [CrossRef]
55. Mbogoro, M.M.; Peruffo, M.; Adobes-Vidal, M.; Field, E.L.; O'Connell, M.A.; Unwin, P.R. Quantitative 3D visualization of the growth of individual gypsum microcrystals: Effect of Ca^{2+}: SO_4^{2-} ratio on kinetics and crystal morphology. *J. Phys. Chem. C* **2017**, *121*, 12726–12734. [CrossRef]
56. Madeja, B.; Avaro, J.; Van Driessche, A.E.; Rückel, M.; Wagner, E.; Cölfen, H.; Kellermeier, M. Tuning the growth morphology of gypsum crystals by polymers. *Cem. Concr. Res.* **2023**, *164*, 107049. [CrossRef]
57. Wagner, M.; Decker, M.; Kunther, W.; Machner, A.; Beddoe, R.E.; Heisig, A.; Heinz, D. Gypsum formation mechanisms and their contribution to crystallisation pressure in sulfate resistant hardened cement pastes during early external sulfate attack at low sulfate concentrations. *Cem. Concr. Res.* **2023**, *168*, 107138. [CrossRef]